TURBULENT FLOW CHARACTERISTICS IN A STENOSED ARTERIAL MODEL WITH RELEVANCE TO ATHEROSCLEROSIS

Sean D. Peterson, Michael W. Plesniak
School of Mechanical Engineering
Maurice J. Zucrow Laboratories, Purdue University
West Lafayette, Indiana 47907 USA
sdpeterson@purdue.edu, plesniak@ecn.purdue.edu

ABSTRACT

The flow field downstream of a nominally concentric 75% axisymmetric area reduction in a tube subjected to a sinusoidal pulsatile waveform is presented herein. The flow field is measured using phase-locked Particle Image Velocimetry at six phase angles. Steady vortical structures are observed in the shear layer from approximately 1.5 tube diameters to 3.7 tube diameters downstream of the stenosis throat. These stationary vortices induce a spatially varying core flow velocity. Additionally, the stenosis creates an annular vortex upstream of the occlusion near the velocity minimum of the pulsatile waveform. These regions of disturbed flow are known to be atherogenic, particularly when the wall shear stress is very low and/or oscillatory.

INTRODUCTION

Cardiovascular diseases, such as atherosclerosis, are the leading cause of death of U.S. citizens over 65 (statistics from the American Heart Association). Atherosclerosis is characterized by altered endothelial and smooth muscle cell physiology in the artery lumen and the subsequent build-up of plaques on the arterial wall. It is known that plaques tend to accumulate and coalesce to form stenoses in regions of low magnitude and/or oscillating wall shear stress. Cells in the region of pathological shear stress distributions respond to the mechanical stimulation by releasing several atherogenic transcription factors and chemical mediators (Topper *et al.*, 1996; Ignarro *et al.*, 2001). Flow distal to a previously formed stenosis can induce non-laminar flow downstream of the constriction, thus inducing pathological shear stress distributions.

Initial research concerning fluid dynamics in stenotic vessels focused upon steady flow conditions. Ahmed and Giddens (1983a, b) measured the flow fields distal to axisymmetric stenoses of 25, 50 and 75% area reduction using laser Doppler anemometry in scaled up models, and Deshpande and Giddens (1980) reported on the turbulence in a constricted tube. These researchers found that distal to a stenosis, there exists a recirculating region and an unsteady, turbulent-like zone. The recirculating zone is a region of low shear stress, while the turbulent-like zone produces unsteady wall shear stresses. Both of these flow conditions are conducive to formation of atherosclerotic lesions. Therefore, a stenosis in an artery further precipitates plaque formation and additional artery occlusion.

Ku (1997), in a review article citing works by Lieber and Giddens (1990), amongst others, states that when the driving flow is pulsatile, the critical upstream Reynolds number for turbulence drops to approximately 300. Lieber and Giddens (1990) reported turbulent flow in a 90% stenosis case during part of the sinusoidal pulsing cycle between 4 and 6 diameters downstream of the stenosis at a mean Reynolds number of 300 and a Womersley number of 5.3. They did not observe turbulence at smaller stenosis degrees. In Ahmed and Giddens' steady flow experiments, they reported that turbulence was produced only for Reynolds numbers greater than 1000 for the 75% stenosis case. Below this Reynolds number, only discrete frequency disturbances, and not breadboard turbulence, were observed.

In the current study, Particle Image Velocimetry (PIV) is used to elucidate the flow field distal to an actual size *in vitro* axisymmetric stenosis model at a moderate physiological Reynolds number and Womersley number in both steady and pulsatile flow. Concurrent numerical simulations by Varghese *et al.* (2003) will be used, in conjunction with companion cellular studies in an identical geometry (see McCann et al., 2002), to correlate regions of mechanical stimulation to cellular response.

EXPERIMENTAL TECHNIQUE AND APPARATUS

Experiments were performed in a custom pulsatile flow facility. A schematic of the flow loop is illustrated in Figure 1. An Ismatec programmable pump controlled by LabView 6.1 software pumped water at 20°C through the facility. The test area consisted of a nominally 10mm ID glass tube with the stenotic test section formed by glassblowing. The axisymmetric 75% area-reduction occlusion had a length-to-diameter ratio of 1.2 and was located 38D

from the tube entrance to ensure fully developed Womersley flow upstream of the test section. The origin of coordinates for downstream measurements is with respect to the throat of the stenosis.

Particle Image Velocimetry, a technique for measuring two component planar velocity fields (see Adrian, 1991; Westerweel, 1993; Willert and Gharib, 1991), was used to measure the velocity fields at the tube centerline in the region from the occlusion to 10 diameters downstream of the stenosis. A sinusoidal voltage waveform was input into the programmable pump. Data were collected at phase angles, φ, of the driving sinusoidal voltage waveform of $\pi/5$, $\pi/2$, $4\pi/5$, $6\pi/5$, $3\pi/2$, and $9\pi/5$. Figure 2 is a plot of the driving waveform with indications of phases at which data were acquired. Due primarily to the fluid inertia in the apparatus, the fluid flow lagged the voltage input by 17.3°, and the amplitude of the bulk flow rate was less than that predicted by an ideal system (no inertia implies that the bulk flow wave form exactly follows the voltage input). The phase lag was determined by fitting a sine curve to peak velocity data during each phase, extracted from the measurements at Z/D = -5. Note that all references to measurement times herein are with respect to voltage, unless otherwise noted. The mean Reynolds number was 1007, with an amplitude of ±480 and a Womersley number of 8.4. In addition to measurements downstream of the stenosis, data were collected 5 diameters upstream of the stenosis at 10 equally spaced phase angles ($n\pi/10$) to determine the inlet flow profiles.

The PIV system consisted of a 50mJ/pulse New Wave GeminiPIV Nd:YAG laser, a TSI PowerView 12-bit, 2000x2000 pixel, cross-correlation CCD array, TSI synchronizer and a dual Pentium Xeon processor data acquisition computer. The TSI Insight 3.53 software package was used to capture and correlate 50 image pairs at each measurement location. The images were correlated using the Hart cross-correlation engine with a bilinear peak-finding algorithm. The primary interrogation was 32x32 pixels with a 16x16 subcorrelation window and a compression ratio of 90%. Each measurement spanned approximately 1.7 diameters of the test section. The physical size of each interrogation region was 0.26x0.26 mm^2 for the primary interrogation window and 0.13x0.13 mm^2 for the subcorrelation window. This provided a spatial resolution (based on the subcorrelation window) of 65 μm. Mean velocity fields were obtained by spatially averaging the 50 instantaneous velocity fields. This relatively small sample size was selected because it offered a good compromise between convergence of the mean field and available disk space. In regions of large cycle-to-cycle flow variations, the small sample size adversely affects the degree of convergence of the mean velocity field.

To alleviate distortion caused by the curved geometry, the test section was submerged in a tank filled with water. This index matching reduced the optical distortions, though it did not eliminate them since there was still a slight index of refraction mismatch between the glass and water. This distortion was small, however, because the glass tube had a relatively thin wall. To reduce the laser reflections off of the glass test section, fluorescent seed particles (Rhodamine 6G, Dichloro-fluorescein), supplied by Johns Hopkins University, were used in conjunction with a narrow bandpass optical filter mounted to the camera. The filter and relatively weak fluorescence of the particles had the negative impact, however, of reducing the signal received by the camera. Though this increased the effect of random pixel noise (*i.e.*, reduced the signal-to-noise ratio), the number of spurious vectors remained quite low (typically much less than 10%), despite the small interrogation regions. Combination of pixel and processing errors at 95% confidence levels lead to uncertainty in mean velocity of ±3% (Moffat, 1988).

RESULTS

The velocity profiles at 10 equally spaced phase angles 5 diameters upstream of the stenosis are compared with the classical Womersley solution in Figure 3 (see Womersley, 1955). The solid black squares correspond to experimental data, while the lines depict the theoretical solution. The data in this figure are the average of ~20 profiles centered at X/D = -5. In Figure 3, the ordinate is the radial location of the measurement point, while the abscissa shows the phase angle in radians. Recall that the phase angle of the measurements is with respect to the input voltage and not the lagging bulk flow. The velocity profiles are normalized by U_{avg}, where $U_{avg}=Re\upsilon/D$. The horizontal dashed lines at each integer value of the abscissa correspond to the zero velocity value for that phase angle and a normalized velocity of 1 for the previous phase angle. The profiles, extracted from the PIV data, are quite similar to the Womersley solution. There are some discrepancies near the wall for some of the profiles, but in general agreement is quite good. The discrepancies are probably causes by the differences between the driving waveform and the actual flow waveform.

Downstream of the stenosis, the flow fields are significantly more complex, with regions of unsteadiness that are both location and phase dependent. Local unsteadiness does not occur during any of the six phase angles measured until approximately 1.3D downstream of the stenosis throat. At this location the Kelvin-Helmholtz instability at the interface of the strong shear layer produces vortical structures. Figure 4 is a plot of mean velocity profiles downstream of the stenosis for all six measured phase angles. The mean velocity profiles are normalized by U_{avg} and are presented in 1D intervals from Z/D = 0 to 10. The indicator dots on the sine curve on the left-hand side of the figure illustrate the approximate time of the measurement along the pulsatile bulk flow velocity waveform. The indicators account for the bulk flow velocity phase lag.

As anticipated, velocity in the near field of the occlusion is characterized by 'plug' flow. Depending on the phase of the flow, this high velocity region diffuses to form regular velocity profiles between Z/D = 5 and 7. Not evident from Figure 4 is that stationary vortical structures exist in the shear layer.

Figure 5 shows the mean flow streamlines from Z/D = 1.2 to 4.8 at phase angles of $\pi/5$, $\pi/2$, $4\pi/5$, $6\pi/5$, $3\pi/2$, and $9\pi/5$, overlaid with flood contours of normalized mean velocity magnitude. Note that the contour levels vary with phase angle to optimize the range of the grey-scale contours. As in the previous figure, the sine wave on the left-hand side of each plot depicts the phase angle of the particular measurement.

Stationary vortices exist at ~2.2D in part a of Figure 5 on both sides of the central high speed flow regions (referred to as the core), with a sense of rotation that suggests that they are part of a steady annular vortex in this region. These vortices are very steady in the instantaneous velocity profiles. Smaller vortices are present at approximately 1.5D, with additional vortical disturbances in the shear layer between 3.5D and 3.7D. Unlike the vortices at 2.2D, which are quite stationary from cycle-to-cycle, these other disturbances move significantly. There is a region between the vortices at 2.2D and 3.5D in which flow near the walls is not recirculatory. Upstream of this location, flow near the wall was entirely retrograde (reversed). The vortices near 3.5D again induce upstream flow near the wall, until eventually the flow reattaches for the final time near Z/D = 4.4. These vortices and the ensuing wavy shear layer affect the core flow by reducing the effective area through which the fluid can pass. This induces alternating regions of high and low velocity between the vortices.

Part b of Figure 5, corresponding to a phase of $\pi/2$, shows clear vortices at Z/D = 2.2. At this phase location, the vortices are not as stationary in the instantaneous images, however. The other vortices present in part a are less clearly defined, however. The mean flow velocity in this phase has accelerated considerably, broadening the disparity in velocity between the core flow and the relatively slow flow near the walls. This creates a practical difficulty in using the PIV technique, inasmuch that to capture the core flow, the time step between frames must be relatively short. Thus, particles in low velocity regions will travel very small distances, thus increasing the uncertainty in these areas. This may account for some of the apparent diffusion of the vortices, though the waviness in the core flow has diminished as well, implying that the affect of the vortices on the flow in the pipe centerline has diminished as the bulk flow velocity peak is approached. The vortices in the 3.5D region have disappeared, and the mean flow field has become quite asymmetric past ~2.5D from the stenosis. Flow on the 'top' surface continues to recirculate, reattaching at about 3.7D, while flow on the 'bottom' surface reattaches directly after the vortex at 2.2D. A similar flow pattern is observed just after the peak waveform in part c of Figure 5, since the fluid has not had much time to adjust to the deceleration of the bulk flow. Asymmetry is possibly a result of the manufacturing of the test section. Holding tight tolerances is not possible with glassblowing, therefore, the occlusion may not be truly concentric with the tube.

In part d of Figure 5, approximately half-way to the minimum velocity peak, the mean flow velocity in the core has decreased substantially (see also Figure 4). The vortex at Z/D = 2.2 is fairly diffuse at this point in the phase, spanning nearly an entire hole diameter in the streamwise direction. The thickness of the recirculation regions has increased substantially, and the near-wall flow field on the 'bottom' surface has changed drastically from that at $\varphi = 4\pi/5$. The near-wall flow on the 'top' surface looks relatively similar, with the recirculation region now extending to ~4.1D. Flow near the 'bottom' surface appears to be influenced by another vortical-like structure near 3.3D. This delays the reattachment point to near that of the upper surface. This vortex at 3.3D could be a resurgence of the vortex in this location reported earlier in the phase.

Near the minimum flow peak, (part e of Figure 5) the flow has decelerated significantly. The vortex at 2.2D is not apparent at this point in the phase. There is a very diffuse vortex-like region near the upper surface, though it is difficult to call this a vortex. Flow near the wall at the upper surface continues recirculating for nearly 4.2 diameters downstream of the stenosis. Flow near the lower surface appears to be affected by both the recirculation region and a vortex centered near 3.4D. Reattachment to the lower surface is difficult to pinpoint, though it appears to occur in the vicinity of Z/D = 4.5. There is an additional flow disturbance not shown in this figure that is *upstream* of the stenosis at Z/D = -0.7 for this phase angle. This upstream vortex does not appear for any of the other phase angles measured. Its formation and evolution remains to be investigated.

The velocity field at the final phase has not been included in Figure 5 for brevity. The mean flow field downstream of the stenosis at $\varphi = 9\pi/5$ is relatively uninteresting. For this case, reattachment of the mean flow field occurs just 0.8D downstream of the stenosis. An annular vortex is present near 0.5D. Downstream of the reattachment, the flow field is all in the streamwise direction.

CONCLUSIONS

Pulsatile flow downstream of an occlusion is quite complex, even at relatively low Reynolds numbers. In this paper, the mean flow field downstream of a 75% area reduction in an axisymmetric tube was presented, for a sinusoidally driven flow with mean Reynolds number of 1007 and Womersley number of 8.4. Stationary vortices exist in the shear layer for a substantial portion of the cycle. Most, though not all, of these vortices vary in position from cycle-to-cycle. Most notable is a very stationary vortex 2.2 diameters downstream of the occlusion at a phase angle of $\pi/5$. A vortex at this position is present for virtually all phase angles measured, however, the vortex tends to move much more at other phase angles. A disturbance in the form of an annular vortex ring was discovered upstream of the stenosis during one of the phase angles corresponding to flow deceleration. These stationary vortices are not present in steady flow conditions. The disturbed flow regions induced by the area constriction impact the wall shear stress, and thus can produce pathological effects *in vivo*. It is, therefore, important to map out regions of

significant flow disturbance to allow future guided research into cellular response.

REFERENCES

Adrian, R.J., 1991, "Statistical Properties of Particle Image Velocimetry Measurements in Turbulent Flow," *Laser Anemometry in Fluid Mechanics vol III* ed R Adrian *et al.* (Lisbon: Ladoani Instituto Superior Tecnico) pp. 115-129.

Ahmed, S.A. and Giddens, D.P., 1983a, "Velocity-Measurements in Steady Flow Through Axisymmetric Stenoses at Moderate Reynolds Number," *J. Biomechanics*, **16(7)**, pp. 505-516.

Ahmed, S.A. and Giddens, D.P., 1983b, "Flow Distrubance Measurements Through a Constricted Tube at Moderate Reynolds Numbers," *J. Biomechanics*, **16(12)**, pp. 955-963.

Deshpande, M.D. and Giddens, D.P., 1980, "Turbulence Measurements in a Constricted Tube," *J. Fluid Mech.*, **97**, pp. 65-89.

Ignarro, L.J., Buga, G.M., Wei, L.H., Bauer, P.M., Wu, G. and del Soldato, P., 2001, "Role of Arginine-Nitric Oxide Pathway in the Regulation of Vascular Smooth Muscle Cell Proliferation," *Proc. Natl. Acad. Sci.*, **98**, pp. 4202-4208.

Ku, D.N., 1997, "Blood Flow in Arteries," *Annu. Rev. Fluid Mech.*, **29**, pp. 399-434.

Lieber, B.B. and Giddens, D.P., 1990, "Post-Stenotic Core Flow Behavior in Pulsatile Flow and Its Effects on Wall Shear Stress," *J. Biomechanics*, **23(6)**, pp. 597-605.

McCann, J.A., Haberstroh, K.M., Frankel, S.H., Plesniak, M.W., Webster, T.J., Wereley, S.T. and Xu, L.X., 2002, "Soluble Proteins Released by Endothelial Cells in Response to Fluid Flow Affect Smooth Muscle Cells," *Fourth World Congress on Biomechanics*, August 4-9, Calgary Canada. (Abstract on CD ROM).

Moffat, R., 1988, "Describing the Uncertainties in Experimental Results," *Exp. Therm. Fluid Sci.*, **1**, pp. 3-17.

Topper, J.N., Cai, J., Falb, D. and Gimbrone, M.A., 1996, "Identification of Vascular Endothelial Genes Differentially Responsive to Fluid Mechanical Stimuli: Cyclooxygenase-2, Manganese Superoxide Dismutase, and Endothelial Cell Nitric Oxide Synthase are Selectively Up-Regulated by Steady Laminar Flow," *Proc. Natl. Acad. Sci.*, **93**, pp. 10417-10422.

Varghese, S., Frankel, S.H., Haberstroh, K.M., Plesniak, M.W., Webster, T.J., Wereley, S.T. and Xu, L.X., 2002, "Numerical Modeling of Pulsatile Turbulent Flows in Stenotic Vessels," *Fourth World Congress on Biomechanics*, August 4-9, Calgary Canada. (Abstract on CD ROM).

Westerweel, J., 1993, "Digital Particle Image Velocimetry - Theory and Application," *PhD Thesis*, Technical University of Delft.

Willert, C. and Gharib, M., 1991, "Digital Particle Image Velocimetry," *Experiments in Fluids*, **10**, pp. 181-193.

Womersley, J.R., 1955, "Method for the Calculation of Velocity, Rate of Flow and Viscous Drag in Arteries when the Pressure Gradient is Known," *J. Physiol.*, **127**, pp. 553-563.

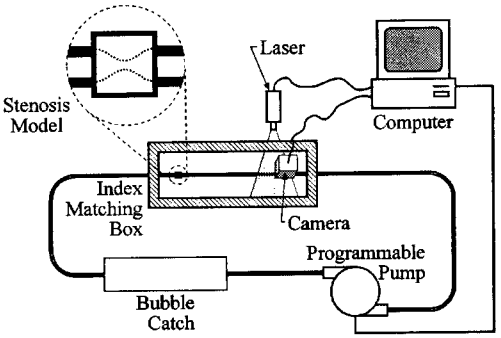

Figure 1: Schematic of Pulsatile Flow Loop.

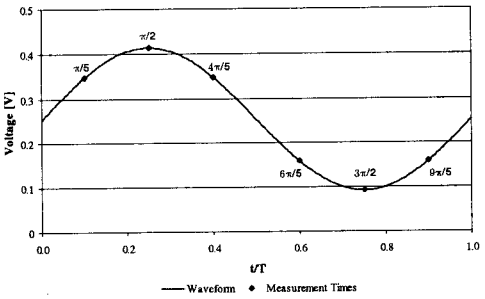

Figure 2: Pulsatile Waveform and Measurement Times

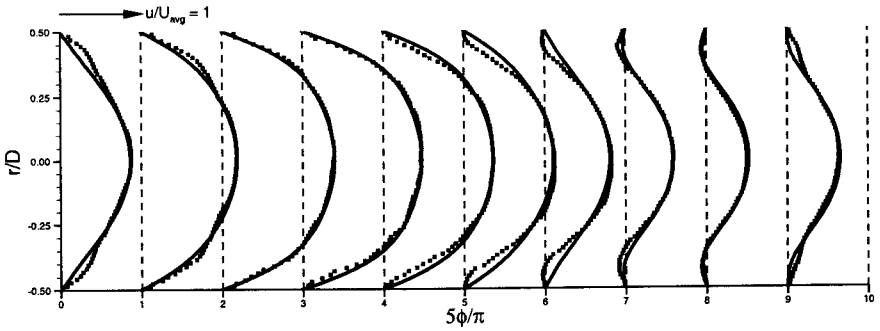

Figure 3: Upstream Velocity Profiles at Various Phase Angles.

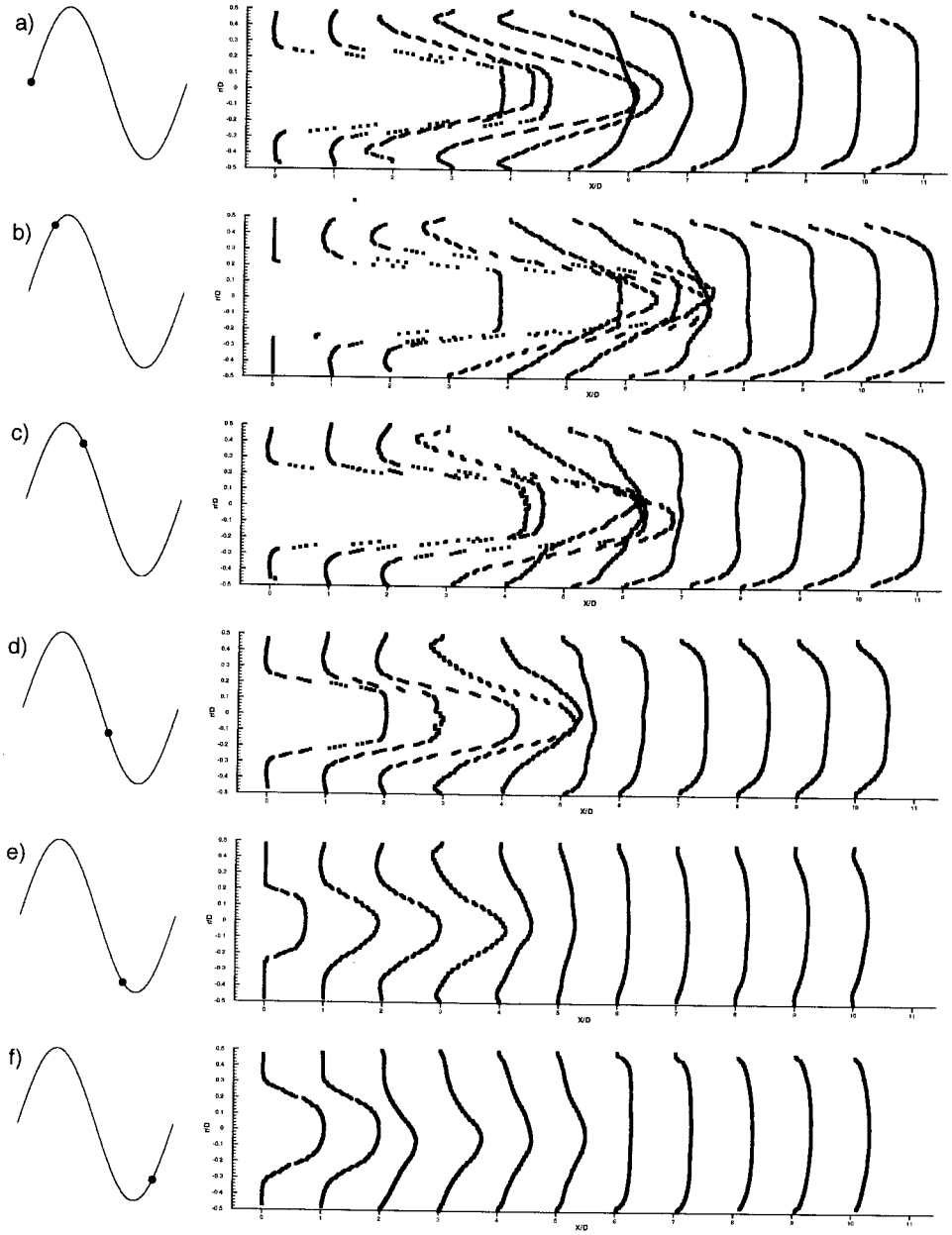

Figure 4: Mean Flow Velocity Profiles Downstream of the Stenosis at Various Phase Angles Indicated by Dots on the Waveform
Phase = a) $\pi/5$ b) $\pi/2$ c) $4\pi/5$ d) $6\pi/5$ e) $3\pi/2$ f) $9\pi/5$.

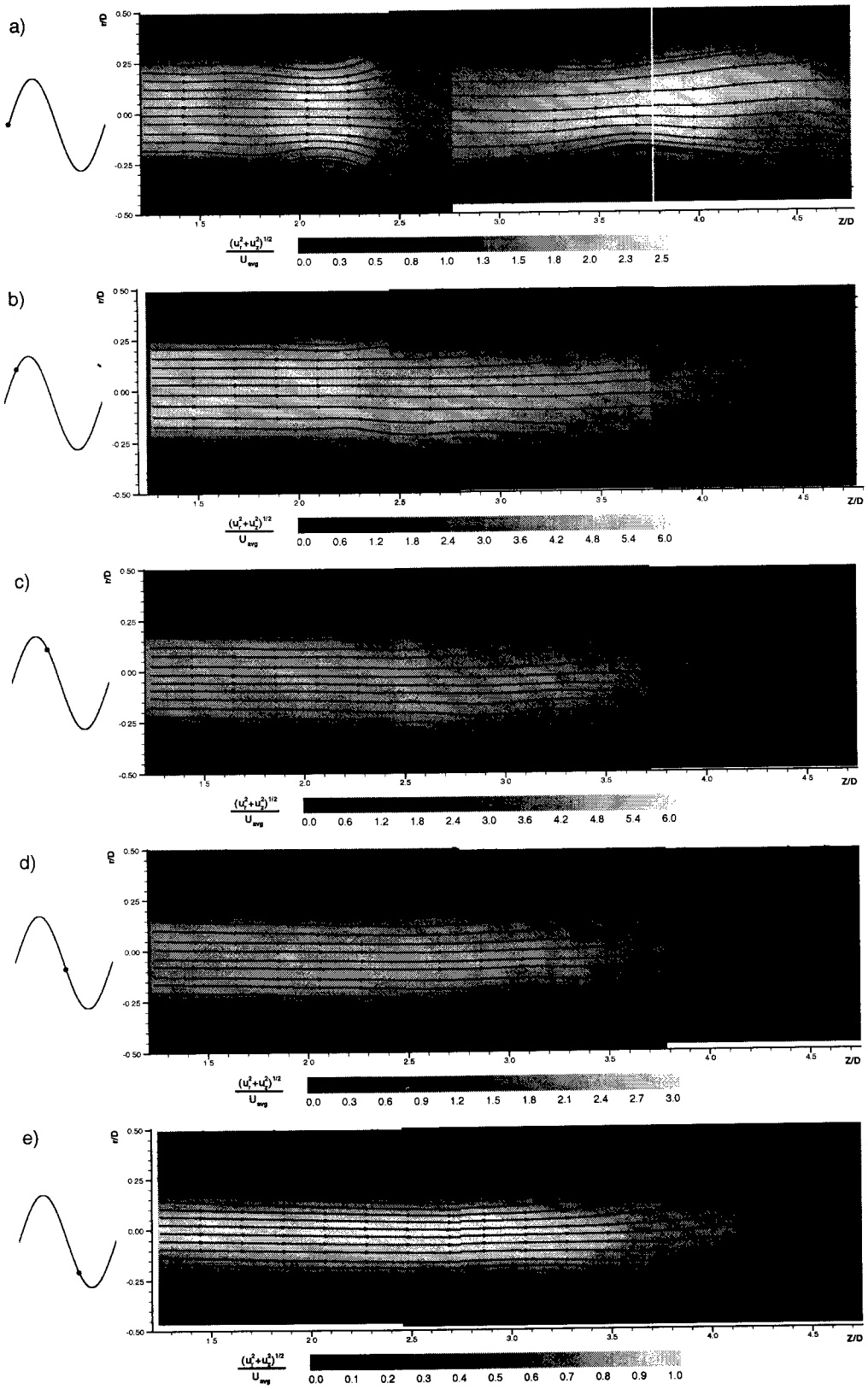

Figure 5: Mean Flow Streamlines with Overlaid Velocity Magnitude
Phase = a) $\pi/5$ b) $\pi/2$ c) $4\pi/5$ d) $6\pi/5$ e) $3\pi/2$.